Viscosity and density decoupling method using a higher order Lamb wave sensor

2014 J. Micromech. Microeng. 24 075002

(http://iopscience.iop.org/0960-1317/24/7/075002)

IOP Publishing Journal of Micromechanics and Microengineering
J. Micromech. Microeng. **24** (2014) 075002 (10pp) doi:10.1088/0960-1317/24/7/075002

Viscosity and density decoupling method using a higher order Lamb wave sensor

Tao Wang[1], **Xiaojing Mu**[2], **Piotr Kropelnicki**[2], **Andrew Benson Randles**[2] **and Chengkuo Lee**[1]

[1] Department of Electrical and Computer Engineering, National University of Singapore, 4 Engineering Drive 3, 117576, Singapore
[2] Institute of Microelectronics (IME), Agency for Science, Technology and Research (A*STAR), 11 Science Park Road, 117685, Singapore

E-mail: elelc@nus.edu.sg

Received 13 December 2013, revised 23 April 2014
Accepted for publication 28 April 2014
Published 22 May 2014

Abstract

Viscosity and density are two important physical parameters of liquid. Such parameters are widely used for label-free chemical detection. Conventional technologies employ acoustic wave sensors to detect viscosity and density. In these sensors, the liquid under test directly contacts with the surface of the sensor. The produced acoustic wave in the sensor leaks to the adjacent liquid layer, causing a shift in the resonance frequency of the sensor. However, such sensors are not able to separately measure the viscosity and density because these two parameters jointly affect the shift of frequency. Although some indirect methods for decoupling these two parameters have been investigated, either dual-device or simultaneous measurement of frequency and attenuation is required. In this paper, a novel AlN based acoustic wave sensor is developed for decoupling viscosity and density. Multiple higher order modes of Lamb waves are generated in this sensor and employed to interact with the adjacent liquid under test. The frequency change of two unique modes (mode C and mode D) has been found in a linear relationship with viscosity and density, respectively. With this unique feature, viscosity and density of a liquid can be distinguished by a single device, which is promising for potential industrial applications, label-free chemical detection and clinical diagnosis.

Keywords: Lamb wave, viscosity, density, decoupling, MEMS sensor

S Online supplementary data available from stacks.iop.org/JMM/24/075002/mmedia

(Some figures may appear in colour only in the online journal)

1. Introduction

Benefiting from advantages of high sensitivity, small size, real-time readout capability, robustness and low cost [1–9], acoustic wave sensors have been developed to sense liquid viscosity (η) and density (ρ) for many years. Acoustic waves, which are normally generated in the device, interact with an adjacent liquid layer that is in contact with the device's surface. Hence, the acoustic wave sensor can sense the liquid mechanical properties directly [10]. Various applications based on the acoustic wave sensors have been successfully developed, such as chemical detection, mixture solution analysis and blood coagulation monitoring [10–15].

However, the main limitation of such acoustic wave sensors is that they are not able to differentiate a liquid's viscosity and density [16, 17]. The frequency response of the acoustic wave sensors is proportional to the square root of viscosity density product [10, 18, 19]. Although many devices have been claimed as viscosity sensors, they actually assume that density is constant and overlook its influence. This assumption may not always be true for real cases [20, 21]. To address such issue, Herrmann *et al* propose an approach using dual surface acoustic wave sensors to decouple two parameters, η and ρ [22]. One reference device with a smooth surface is used to sense $(\eta \cdot \rho)^{1/2}$. The other device is corrugated by microfabricated sagittal trenches. The frequency response

of the corrugated sensor is proportional to ρ and nearly non-sensitive to η. η, then can be calculated from known $(\eta \cdot \rho)^{1/2}$ and ρ. The main drawback of this approach is the employment of a dual-device, which significantly increases the cost and complexity. Challenges also come from the indirect differentiation method, making the signal processing difficult. Another attempt to decouple the two parameters was reported by Martin *et al* using a Lamb wave sensor [23]. Because the frequency related phase velocity of Lamb waves is mainly influenced by liquid density, the frequency response of this sensor is found to be proportional to ρ in a relatively wide range of viscosity. On the other hand, the attenuation response of this sensor still depends on $(\eta \cdot \rho)^{1/2}$. With measured ρ and $(\eta \cdot \rho)^{1/2}$, η hence can be derived. Although this approach realizes the separation of η and ρ with a single device, it is still an indirect method and the accuracy of attenuation measurement is not guaranteed. In addition, the phase velocity of Lamb waves is not solely determined by liquid density. This device can only function when liquid viscosity is small and the influence of liquid sound velocity is neglected. Zhou *et al* made an improved Lamb wave sensor, which successfully decoupled the liquid sound velocity using multi-mode Lamb waves. The remaining problems associated with the Lamb wave sensor are not yet addressed [24].

Another limitation is from the widely adopted delay line configuration [24–26]. Although the Lamb wave sensor is a powerful device for liquid sensing [27–31], the delay line configuration has issues of low quality factor, low stability and low reproducibility. On the contrary, a resonator configuration provides a compact and rugged solution with a high quality factor, which significantly reduces the complexity of signals read out [10]. Unfortunately, studies on Lamb wave resonators for liquid sensing are quite limited [32, 33]. In addition, most researchers mainly focus on the lowest mode of Lamb wave and pay no attention to the higher order modes effects on liquid properties sensing at all.

In this paper, we propose a novel AlN based MEMS Lamb wave sensor, which is able to directly measure a liquid's η and ρ by using higher order modes of Lamb wave. This unique feature realizes the easy separation of η and ρ by a single device for the first time. A resonator configuration is utilized to guarantee stable and easy-readout signals. Experimental results prove the sensor's capability of differentiating liquids like DI water and ethanol, which are likely to be mixed up when using a conventional method.

2. Design of the viscosity and density decoupled sensor

When a Lamb wave sensor is loaded with a liquid, the phase velocity of its lowest asymmetric mode A_0, which is commonly employed for liquid sensing by conventional sensors, is given by [26]:

$$V_{\mathrm{ph}} = \frac{2\pi}{\lambda}\sqrt{\frac{B}{M_{\mathrm{eff}}}} \tag{1}$$

where λ is the wavelength of the acoustic wave, B the bending stiffness of the plate ($B = d^3E/[12(1-\upsilon^2)]$), d is the plate thickness, E is the Young's modulus, υ is the Poisson ratio. M_{eff} is the effective mass:

$$M_{\mathrm{eff}} = M_{\mathrm{plate}} + M_{\mathrm{den}} + M_{\mathrm{vis}} \tag{2}$$

M_{plate} is the unit plate mass, M_{den} is the mass loading due to liquid density, and M_{vis} is the viscous loading of the liquid. The corresponding frequency is expressed as:

$$f = \frac{v_{\mathrm{ph}}}{\lambda}. \tag{3}$$

The A_0 wave is a combination of longitudinal and transverse waves, where the motion of the particles on the plate is elliptical, having components both perpendicular and parallel to the plate plane. The normal component along y-direction generates an evanescent pressure wave that displaces the liquid in the skin depth, and liquid mass loading M_{den} lowers the phase velocity. Meanwhile, the in-plane component along x-direction generates shear waves in liquid. The viscous loading contributes to the M_{vis} and lowers the phase velocity as well [23].

According to [34], the relative magnitude of the two components is a function of frequency–thickness product. At a certain product value, one of the components becomes zero and the motion of the particles is either entirely perpendicular or parallel to the plate plane. Especially for the higher order modes of Lamb wave, at nascent frequencies of some particular modes, the motion of the particles at the backside surface is either entirely perpendicular or parallel to the plate plane. The mode with perpendicular motion should thus be only sensitive to ρ, while the mode with parallel motion should respond to η. η and therefore ρ can be separately determined by using the two unique modes.

However, the frequency of higher order modes may be extremely high. In [35], authors reported the first four modes with frequencies up to 4 GHz. Such high frequency will cause extra issues for signal readout and processing. In addition, high frequency is not preferred for viscosity sensing, as liquids are more likely to become viscoelastic at a high frequency range. The viscoelastic effect will be discussed in section 4.3.2. According to the velocity dispersion curves, the phase velocity of the Lamb wave decreases on increasing the plate thickness, which leads to a lower frequency. Therefore, a relatively thick plate is usually adopted to decrease the frequency of the higher order modes.

A schematic drawing of the viscosity and density decoupled sensor is shown in figure 1. A 2 μm AlN layer is adopted as the piezoelectric material due to its CMOS compatible process. This material has been well studied and widely utilized in acoustic wave resonators because of its efficient electromechanical transaction [36]. A set of interdigital transducer (IDT) electrodes made of 0.6 μm Al with 10 μm periodicity ($= \lambda/2$) is used for Lamb wave generation. Since the plate is not infinite, propagating Lamb waves will be reflected back at the lateral extremities, giving rise to resonant modes [37]. It is significant that a 30 μm Si layer and a 1.4 μm SiO_2 layer are attached below the AlN layer. This AlN/Si/SiO_2 composite plate has a thickness of 33.4 μm in total, which is about 1.5 times the Lamb wavelength 20 μm. Equation (1) is no longer valid for such situation because it

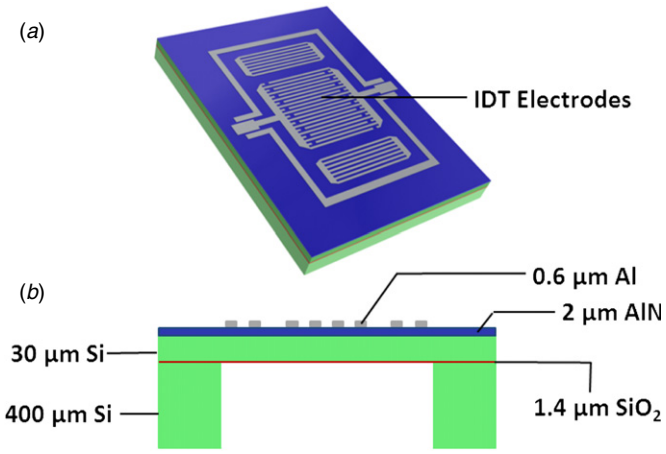

Figure 1. Schematic drawing of the directly decoupled viscosity and density sensor: (*a*) bird's view and (*b*) cross-sectional view. The IDT electrodes induce the Lamb wave within the plate. Relatively thick device silicon (30 μm) is employed for the plate to lower the frequency of higher order modes.

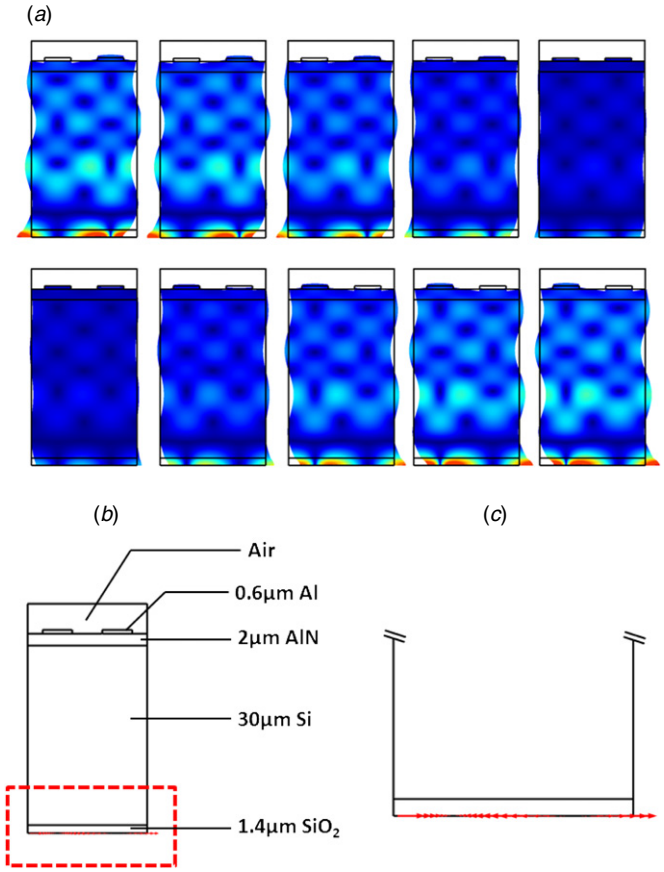

Figure 2. Simulation results of mode 1: (*a*) mode shape; (*b*) velocity vectors on backside surface and; (*c*) zoom-in view of velocity vectors. Motion of the particles on the backside surface is entirely in-plane, generating shear waves in liquid.

is only valid when $d \ll \lambda$ [26]. A 2D finite element model therefore is employed for analysis in this work.

Admittance and resonance mode shapes of higher order modes are simulated using COMSOL multi-physics software. Only those modes which can be excited are considered. Two noteworthy modes are found in the

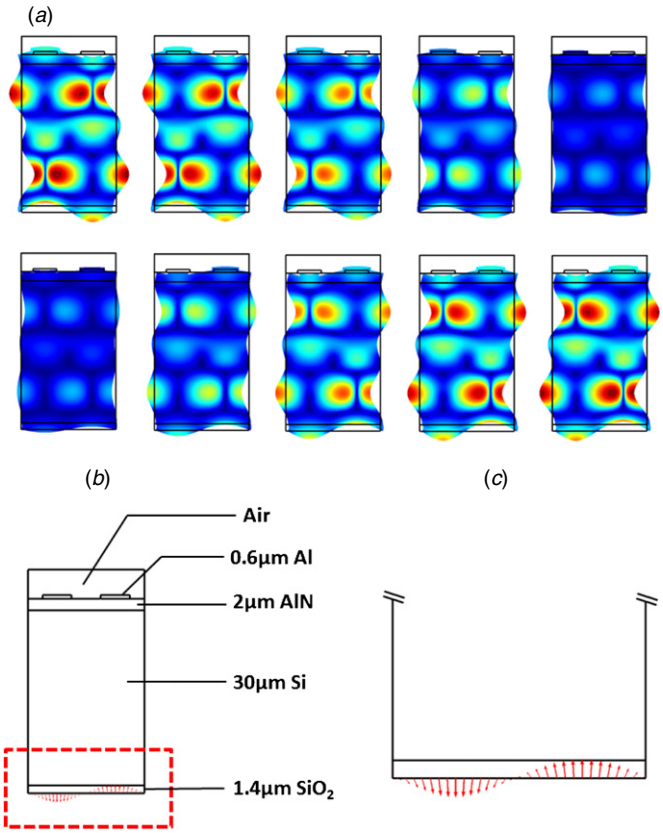

Figure 3. Simulation results of mode 2: (*a*) mode shape; (*b*) velocity vectors on backside surface and; (*c*) zoom-in view of the velocity vectors. Motion of the particles on the backside surface is out-of-plane, generating longitudinal waves in liquid.

simulation, denoted as mode 1 and mode 2. The shape of mode 1 is shown in figure 2(*a*) (see supplementary data available at stacks.iop.org/JMM/24/075002/mmedia) and the velocity vectors of the backside surface are shown in figures 2(*b*) and (*c*). The motion of the backside surface is in-plane and velocity vectors are entirely parallel to the plate plane without any normal components. For mode 2, the motion of the backside surface is out-of-plane, as shown in figure 3(*a*) (see supplementary data available at stacks.iop.org/JMM/24/075002/mmedia). As can be seen from figures 3(*b*) and (*c*), most of the velocity vectors are perpendicular to the plate plane. Non-perpendicular vectors are rare and weak, and their influence is quite limited. As aforementioned, mode 1 with parallel motion can be used to sense viscosity, while mode 2 with perpendicular motion can be used to sense the density of a liquid.

To further study the two modes, a layer of fluid is defined at the bottom of the device. The interface 'acoustic–piezoelectric interaction' with frequency domain study is employed to simulate the interaction between the device and fluid. It is worth noting that the fluid is modeled as 'viscous', which takes both the fluid's density and viscosity into consideration. However, due to software limitations, viscosity lowers the peak amplitude but does not influence the frequency at all. Only the density contributes to the frequency shift of the device. Simulated frequency responses to change in density of mode 1 and 2 are shown in figure 4. Behaviors of these two modes

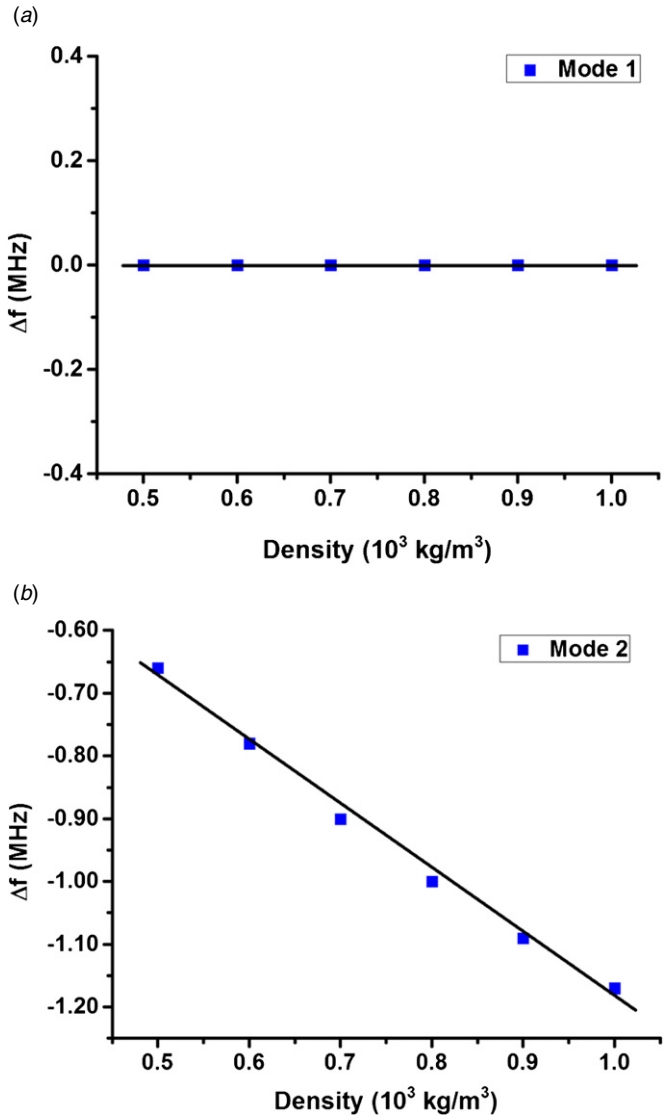

Figure 4. Simulated relative frequency shifts to the density of (*a*) mode 1 and (*b*) mode 2. Frequency of mode 1 does not shift due to density at all, which can be used for viscosity sensing.

are much different. The frequency of mode 1 does not shift at all, while the frequency of mode 2 decreases with a sensitivity of $-$ 2478 ppm g^{-1} cm^{-3}. Such simulation results prove that liquid density has no influence on the frequency shift of mode 1, thus any frequency shift of mode 1 should be contributed by viscosity.

3. Device fabrication

The fabrication process sequence of the Lamb wave viscosity and density sensor is illustrated in figure 5. Fabrication starts from an 8″ silicon-on-insulator (SOI) (1 0 0) wafer with a 30 μm silicon device layer, a 1.4 μm buried oxide (BOX) layer and a 600 μm thickness handle silicon layer. Initially physical vapor deposition (PVD) is used to grow a 2 μm AlN piezoelectric layer on the SOI wafer at a deposition rate of 500 Å min^{-1}. Then a 600 nm Al layer is deposited by e-beam evaporation and patterned to form IDT electrodes by reactive-ion etching (RIE) with an etching rate of 7200 Å min^{-1}.

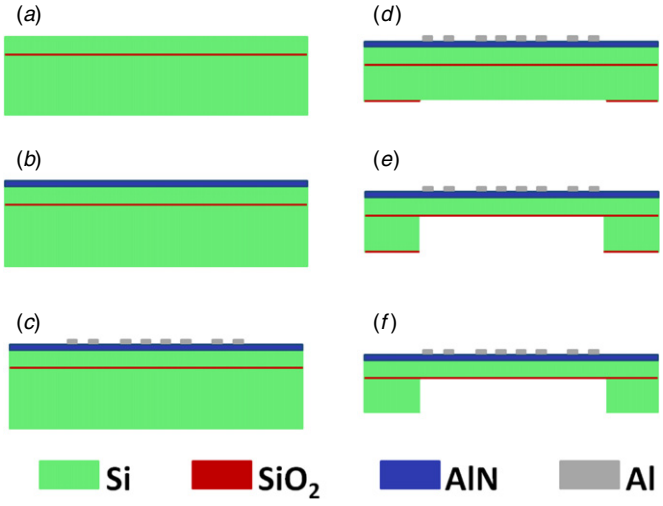

Figure 5. Fabrication process flow of the device: (*a*) SOI substrate with 30 μm device silicon layer; (*b*) deposition of 2 μm AlN layer using PVD; (*c*) Al metal deposition and pattering to form IDT electrodes; (*d*) wafer thinning to 600 μm, followed by 1.5 SiO_2 hard mask deposition and pattering on backside; (*e*) backside Si DRIE release; (*f*) SiO_2 hard mask removal by wet etching.

After the front side process, the wafer is thinned down to a thickness of 400 μm by mechanical grinding. Next, a 1.5 μm PECVD SiO_2 layer is deposited on the backside of the wafer as a hard mask for the release process, which is patterned by RIE. The Si substrate is etched by deep RIE down to the BOX layer to release the membrane structure. Finally, the SiO_2 hard mask is removed using wet etching.

The fabricated device is shown in figure 6. Both optical microscope and scanning electron microscope (SEM) images indicate the well patterned electrodes. The bright regions between electrodes in figure 6(*b*) are probably due to electrons charging on the AlN dielectric layer. A cross-sectional SEM image of the device is given in figure 6(*c*).

4. Experimental results and discussions

4.1. Testing setup

The fabricated device is mounted on a PCB with a through hole (3 mm in diameter) in the center, as shown in figures 7(*a*) and (*c*). This hole enables the backside surface of the released membrane to be exposed to the environment. Liquid under test is injected through the hole and contacts with the bottom surface. All the bonding wires are sealed and protected by silicone, as illustrated in figure 7(*b*). Silicone sealing prevents bonding wires from the possible influences of splashed liquid or external materials. Even a small amount of liquid on bonding wires can result in a significant signal fluctuation due to the perturbation on parasitic parameters such as capacitance. Hence, silicone sealing is a key step to ensure the stable signals. Furthermore, to eliminate the parasitic effects brought by PCB package and cables, a PCB calibration kit with open, short, through and load (50 Ω) configurations is fabricated as well, as shown in figure 7(*d*). These configurations have exactly the same layout as the test PCB package.

The testing is conducted by measuring the S11 parameter in the range of 400 to 550 MHz using an Agilent E5071B

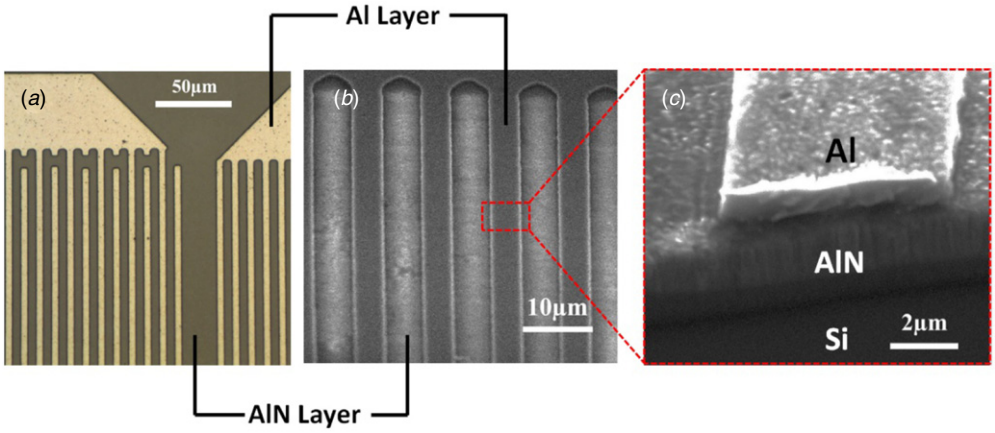

Figure 6. The fabricated decoupled viscosity and density sensor: (*a*) optical microscope photograph; (*b*) scanning electron microscope (SEM) photograph; and (*c*) cross-sectional SEM photograph.

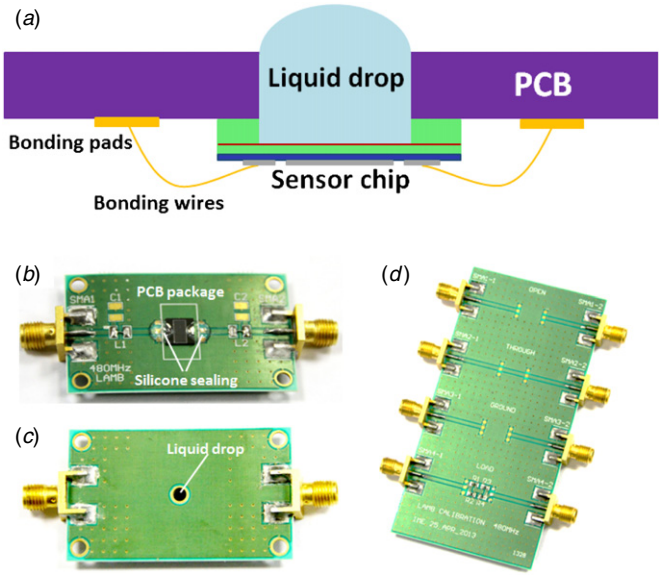

Figure 7. (*a*) Schematic drawing of packaged sensor with loaded liquid under test; sensor mounted on the holed PCB with sealed bonding wires by silicone (*b*) front side and (*c*) backside; (*d*) PCB calibration kit for eliminating the interferences from cables and PCB package.

network analyzer under a fixed room temperature of 24 °C. The maximum sweeping points of this instrument is 16001, which implies that the frequency resolution is limited to about 10 kHz. Calibration is first performed with the kit mentioned above. The open circuits S11 after calibration is greater than −5 dB. This indicates that most of signals are reflected back and interference from PCB and cables is minimized.

4.2. Device testing in air

The S11 parameter in air is first recorded as in figure 8 for the reference, and all shifted frequencies are compared with this. Benefitting from a thick stack plate, five higher order Lamb wave modes are generated within the 150 MHz bandwidth. In addition, high quality factors improve the accuracy of the frequency shift measurement and make easy-readout possible.

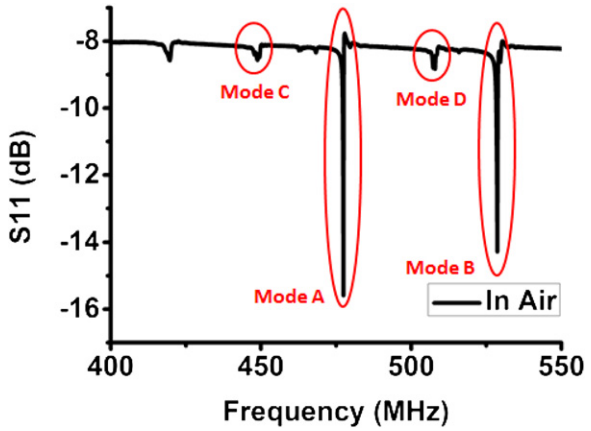

Figure 8. S11 parameter in the range of 400 to 600 MHz, measured in air using an Agilent E5071B network analyzer. The signal is quite stable while the high Q-factor makes easy and accurate frequency determination possible.

Table 1. Summary of the mechanical properties of air, DI water, acetone, ethanol and IPA.

Samples	η (mPa s)	ρ ($\times 10^3$ kg m^{-3})	$(\eta \cdot \rho)^{1/2}$ (kg m^{-2} s$^{-1/2}$)
Air	0.019	0.001	0.005
DI water	0.894	1.000	0.946
Acetone	0.306	0.791	0.492
Ethanol	1.070	0.789	0.921
IPA	1.960	0.786	1.241

4.3. Liquid testing

4.3.1. Liquid testing using DI water, acetone ethanol and IPA. Four liquid samples are adopted for the testing: DI water, acetone, ethanol and IPA. Mechanical properties (viscosity η, density ρ and square root viscosity–density product $(\eta \cdot \rho)^{1/2}$) of the four liquids are summarized in table 1. Each liquid is dripped into the PCB hole (shown in figure 7(*c*)) and directly contacts the backside surface of the sensor. When the signal is stable with no fluctuation, the S11 parameter is recorded.

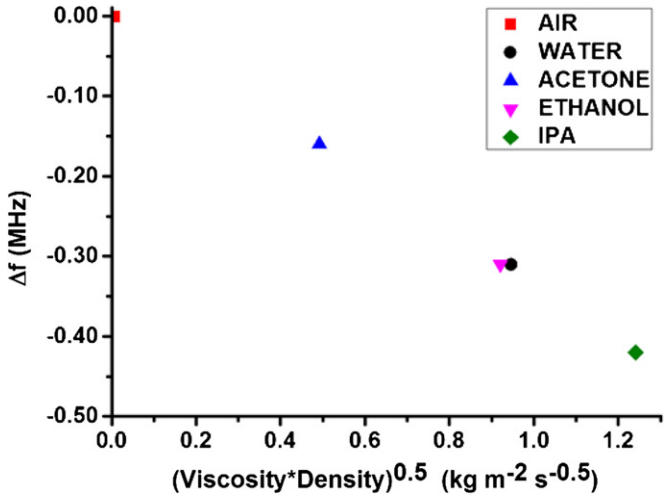

Figure 9. Relative frequency shifts to the square root of viscosity-density product of mode A in DI water, acetone, ethanol and IPA. DI water and ethanol share the same frequency response.

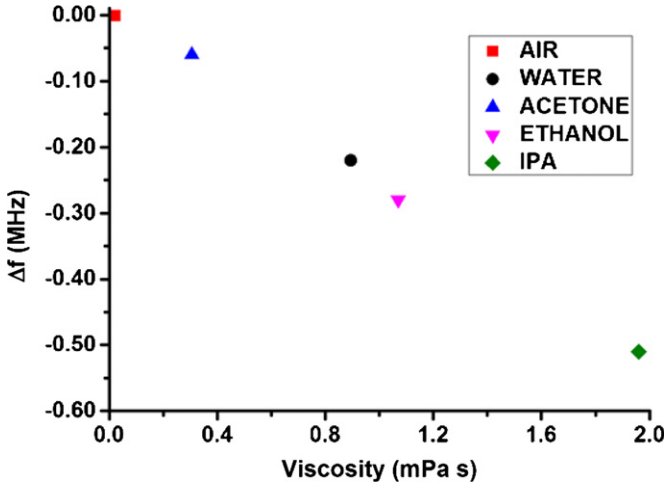

Figure 10. Relative frequency shifts to the viscosity of mode C in DI water, acetone, ethanol and IPA. DI water and ethanol are discriminated due to their different viscosities.

Frequency responses of all five modes are studied, and four of them are noteworthy, denoted as modes A to D.

The frequency responses of modes A and B behave similarly, and a linear correlation between frequency and $(\eta \cdot \rho)^{1/2}$ is revealed. Such behavior is similar to the conventional sensors. The frequency response of mode A is plotted in figure 9 as an example. These two modes are not able to differentiate the coupled influence of viscosity and density. Although DI water and ethanol have different viscosities and densities, their products are very close to each other (as shown in figure 9). The two liquids therefore can hardly be differentiated using these conventional modes. Figure 10 shows the frequency response of mode C, which behaves like mode 1 in simulation (see figure 2). This mode reveals an almost linear frequency shift relationship with the η of liquids, without the influence of density change. Thus, DI water and ethanol are clearly distinguished due to the viscosity difference. On the contrary, the frequency response of mode D seems sensitive to ρ only, corresponding to mode 2 in simulation (see figure 3). Acetone, ethanol and IPA have almost the same ρ but largely different η. As is demonstrated in figure 11, the frequency responses these three liquids overlap, indicating that mode D is non-sensitive to η. As a result, viscosity and density of a liquid are separately detected by using modes C and D, while the corresponding viscosity and density sensitivity are calculated as -569 ppm mPa s^{-1} and $-$ 748 ppm g^{-1} cm^{-3}, respectively.

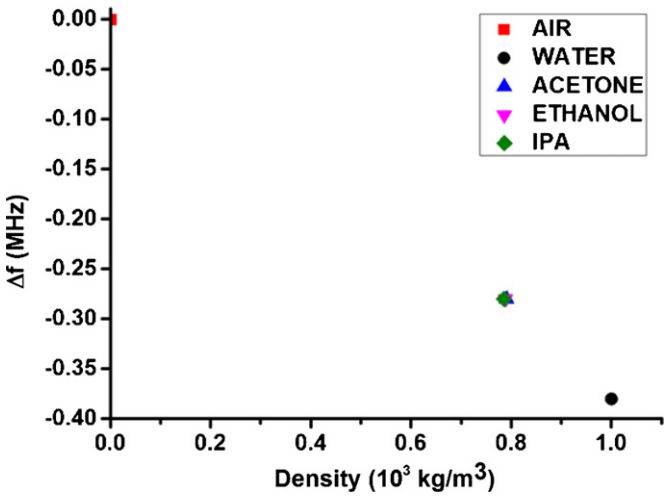

Figure 11. Relative frequency shifts to the density of mode D in DI water, acetone, ethanol and IPA. Acetone, ethanol and IPA cannot be differentiated because of the almost same density, indicating that the frequency response of mode D is not influenced by viscosity.

Table 2. Summary of the mechanical properties of glycerol–water mixtures.

Glycerol volume concentration (%)	η (mPa s)	ρ ($\times 10^3$ kg m^{-3})	$(\eta \cdot \rho)^{1/2}$ (kg m^{-2} s$^{-1/2}$)
0	0.894	1.000	0.946
10	1.221	1.029	1.121
20	1.732	1.060	1.354
30	2.575	1.089	1.673
40	4.058	1.118	2.130
50	6.879	1.144	2.806

4.3.2. Liquids testing using glycerol–water mixtures. To further characterize the sensor performance in the high-viscosity range, glycerol–water mixtures are utilized. Glycerol–water solutions, as standard Newtonian liquids, are widely used for viscosity sensor testing. By changing the glycerol/water ratio, the viscosity of these solutions ranges from 1 to 1500 mPa s at room temperature, while the density only changes from 1 to 1.29 g cm^{-1} [38]. Mixtures with glycerol volume concentration from 0 to 50% are made for testing, using G5516 glycerol ($\geqslant$99%) from Sigma-Aldrich®. Viscosity η, density ρ and square root viscosity–density product $(\eta \cdot \rho)^{1/2}$ of the glycerol–water mixtures are calculated and summarized in table 2.

Table 3. Summary of the mechanical properties of NaCl solutions.

NaCl mass concentration (%)	η (mPa s)	ρ ($\times 10^3$ kg m^{-3})	$(\eta \cdot \rho)^{1/2}$ (kg m^{-2} s$^{-1/2}$)
0	0.894	1.000	0.946
4.76	0.959	1.040	0.998
9.09	1.042	1.068	1.055
13.04	1.142	1.095	1.119
16.67	1.260	1.132	1.195
20.00	1.396	1.157	1.271

Highly viscous liquids like glycerol–water mixtures tend to deviate from Newtonian behavior, becoming viscoelastic. The response of most viscosity sensors departs from the linear dependence when liquid viscosity goes beyond a certain value due to the viscoelastic effect [39]. For example, the response of the device reported in [40] starts becoming nonlinear from about 3.6 mPa s. This turning point is related to the device operating frequency, which becomes higher for lower frequency. In terms of the current work, a fully linear correlation of mode C is observed in figure 12(*b*), with liquid viscosity up to 7 mPa s. Such linear behavior may be partially due to the moderate operating frequency. Further investigation will be conducted in our future work. It is also worth noting that although the liquid viscosity changes a great deal, the frequency shift of mode D is very small and proportional to the slightly changed density, as shown in figure 12(*c*). No deviation from the linear dependence is observed, implying that mode D is highly independent of liquid viscosity.

4.3.3. Liquids testing using NaCl solutions. NaCl solutions with different concentrations are also made for testing, by dissolving 0.5–2.5 g NaCl into 10 ml DI water. Volume changes due to dissolved NaCl are considered for calculation as well. Both viscosity and density of NaCl solution slightly increase with NaCl concentration, summarized in table 3 [41]. NaCl solutions are mainly used to study the minimum detection limit of this decoupled viscosity and density sensor. The frequency shifts due to NaCl solutions are extremely small. Such small shifted frequency already approaches to the frequency resolution of network analyzer, illustrated in figure 13. Minimum detectable viscosity and density changes of this sensor are 0.065 mPa s and 0.025 g cm^{-3}, respectively.

4.4. Potential applications as a label-free liquid sensor

As mentioned above, conventional acoustic wave sensors have many limitations when used as label-free liquid sensors. The frequency responses to liquids like DI water and ethanol probably overlap, as shown in figure 9. Such liquids may be determined as being the same one by conventional sensors. Whereas, with the decoupled viscosity and density sensor, a novel 2D method for label-free liquid detection is available by plotting the frequency response of mode C versus that of mode D, as demonstrated in figure 14. In this plot, DI water and ethanol can be easily differentiated because of their different viscosities and densities. Acetone, ethanol and IPA share almost the same density and form a horizontal line in

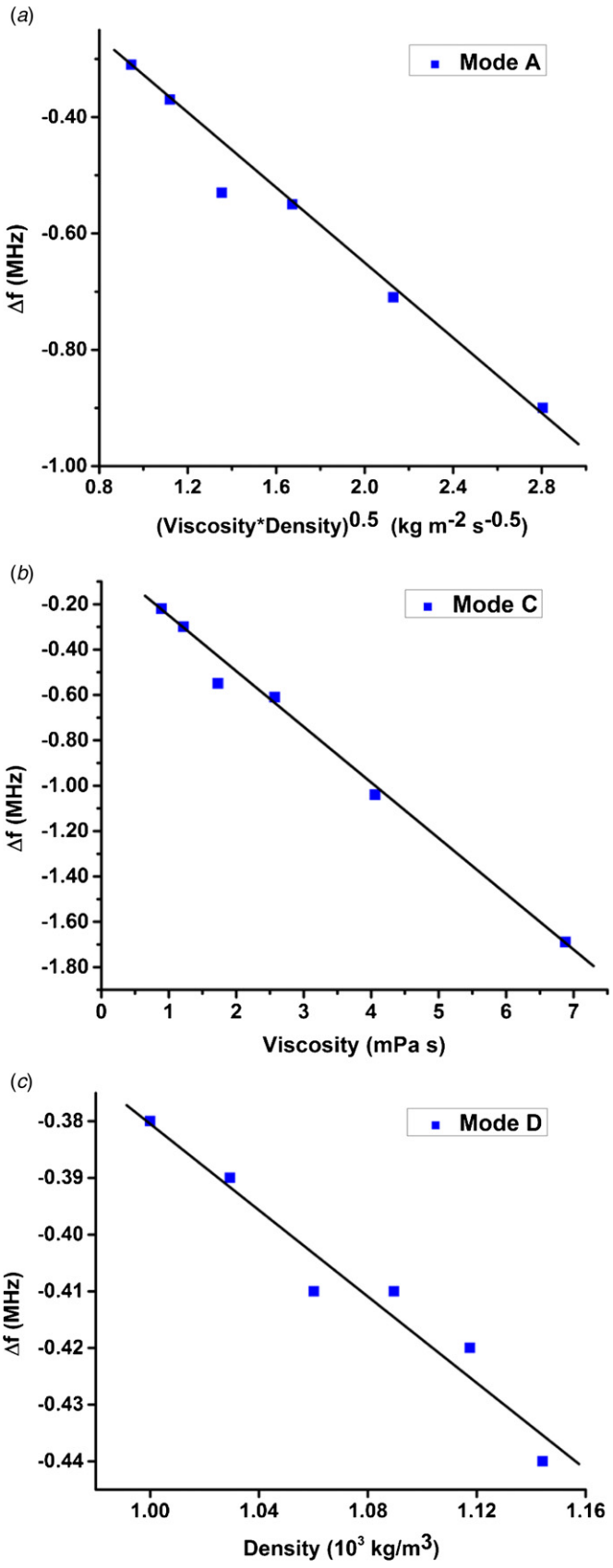

Figure 12. Relative frequency shifts in glycerol–water solutions with volume concentration from 0% to 50%: (*a*) mode A to the square root of viscosity-density product; (*b*) mode C to the viscosity and; (*c*) mode D to the density.

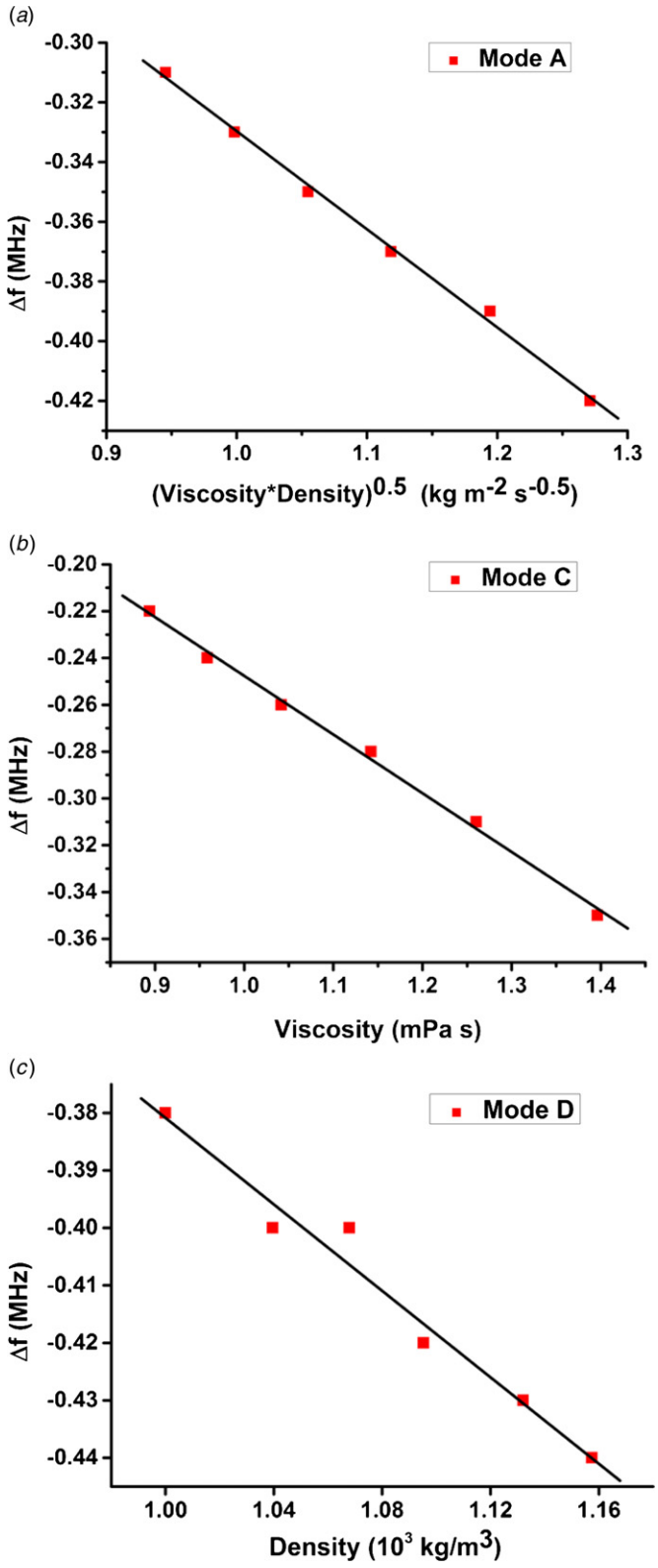

Figure 13. Relative frequency shifts in NaCl–water solutions with mass concentration from 0% to 20%: (*a*) mode A to the square root of viscosity-density product; (*b*) mode C to the viscosity and; (*c*) mode D to the density.

the plot. This 2D method may have wide applications in the oil industry. Diesel fuels with different cetane numbers have relatively constant density but varying viscosity likewise [22].

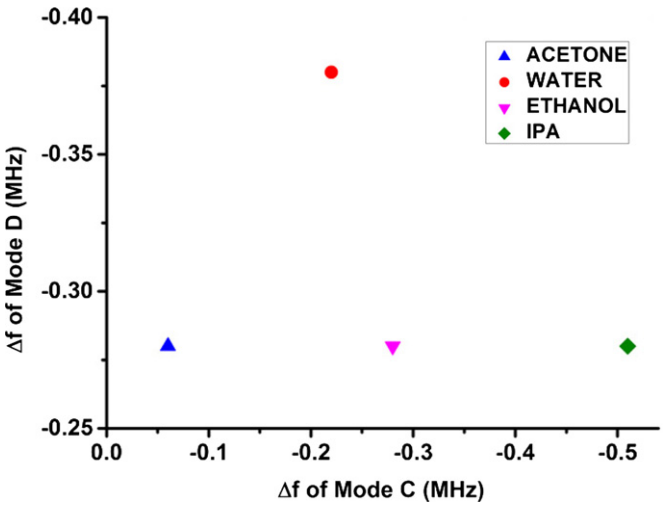

Figure 14. A novel 2D method for label-free liquid detection. Frequency responses of mode C and mode D are plotted in *X*-axis and *Y*-axis, respectively. Liquids with the same viscosity–density product or the same density can be easily discriminated by this method.

The cetane number thus can be determined by measuring the viscosity. Meanwhile, if diesel fuel is unexpectedly mixed into water, it should be detected due to the density difference. By using this 2D method, cetane number and water percentage may be obtained simultaneously. Other applications of the 2D method in the oil industry will be further explored in the future.

5. Conclusion

In this paper, a directly decoupled viscosity and density sensor using a Lamb wave resonator is proposed. The AlN MEMS resonator based sensor is capable of generating stable signals with high quality factor. Higher-order modes of Lamb wave are utilized for viscosity and density detection. Two unique modes (mode C and mode D) are found with backside surface particle motion either parallel (mode C) or perpendicular (mode D) to the plate plane. The frequency response of mode C is dominated by viscosity with a sensitivity of -569 ppm mPa s^{-1}, while that of mode D is solely determined by density with a sensitivity of -748 ppm g^{-1} cm^{-3}. Decoupled viscosity and density sensing is achieved by single device. Without suffering from viscoelastic effects, the viscosity dependence of this sensor remains linear with liquid viscosity up to 7 mPa s. The minimum detectable changes of viscosity (0.065 mPa s) and density (0.025 g cm^{-3}) are quite small. A novel 2D liquid detecting method based on the sensor is proposed. DI water and ethanol are clearly differentiated by this method. Potential applications of such a 2D method in the oil industry are shown as well.

Acknowledgment

This work was supported in part by the Agency for Science, Technology and Research (A*STAR) under Science and

Engineering Research Council (SERC) grants 1021650084 and 1220103064.

References

[1] Cole M, Sehra G, Gardner J W and Varadan V K 2004 Development of smart tongue devices for measurement of liquid properties *IEEE Sensors J.* **4** 543–50

[2] Fu Y Q, Luo J K, Du X Y, Flewitt A J, Li Y, Markx G H, Walton A J and Milne W I 2010 Recent developments on ZnO films for acoustic wave based bio-sensing and microfluidic applications: a review *Sensors Actuators* B **143** 606–19

[3] Voiculescu I and Nordin A N 2012 Acoustic wave based MEMS devices for biosensing applications *Biosens. Bioelectron.* **33** 1–9

[4] Rapp B E, Gruhl F J and Lange K 2010 Biosensors with label-free detection designed for diagnostic applications *Anal. Bioanal. Chem.* **398** 2403–12

[5] Latif U, Mujahid A, Afzal A, Sikorski R, Lieberzeit P A and Dickert F L 2011 Dual and tetraelectrode QCMs using imprinted polymers as receptors for ions and neutral analytes *Anal. Bioanal. Chem.* **400** 2507–15

[6] Cooper M A 2003 Label-free screening of bio-molecular interactions *Anal. Bioanal. Chem.* **377** 834–42

[7] Lange K, Rapp B E and Rapp M 2008 Surface acoustic wave biosensors: a review *Anal. Bioanal. Chem.* **391** 1509–19

[8] Priego Capote F and Luque de Castro M D 2007 Ultrasound in analytical chemistry *Anal. Bioanal. Chem.* **387** 249–57

[9] Olfatnia M, Shen Z, Miao J M, Ong L S, Xu T and Ebrahimi M 2011 Medium damping influences on the resonant frequency and quality factor of piezoelectric circular microdiaphragm sensors *J. Micromech. Microeng.* **21** 045002

[10] Nomura T, Saitoh A and Horikoshi Y 2001 Measurement of acoustic properties of liquid using liquid flow SH-SAW sensor system *IMCS-8'08: 8th Int. Meeting on Chemical Sensors (Switzerland, 2–5 July 2000)* pp 69–73

[11] Yamazaki T, Kondoh J, Matsui Y and Shiokawa S 2000 Estimation of components and concentration in mixture solutions of electrolytes using a liquid flow system with SH-SAW sensor *Sensors Actuators* A **83** 34–9

[12] Vivancos J-L, Racz Z, Cole M and Gardner J W 2012 Surface acoustic wave based analytical system for the detection of liquid detergents *Sensors Actuators* B **171–172** 469–77

[13] Xu W, Appel J and Chae J 2012 Real-time monitoring of whole blood coagulation using a microfabricated contour-mode film bulk acoustic resonator *J. Microelectromech. Syst.* **21** 302–7

[14] Viswanath A, Green S R, Kosel J and Gianchandani Y B 2013 Metglas–Elgiloy bi-layer, stent cell resonators for wireless monitoring of viscosity and mass loading *J. Micromech. Microeng.* **23** 025010

[15] Huang X *et al* 2013 A MEMS differential viscometric sensor for affinity glucose detection in continuous glucose monitoring *J. Micromech. Microeng.* **23** 055020

[16] Mitsakakis K, Tsortos A, Kondoh J and Gizeli E 2009 Parametric study of SH-SAW device response to various types of surface perturbations *Sensors Actuators* B **138** 408–16

[17] Oita I, Halewyck H, Thys B, Rombaut B, Vander Heyden Y and Mangelings D 2010 Microfluidics in macro-biomolecules analysis: macro inside in a nano world *Anal. Bioanal. Chem.* **398** 239–64

[18] Da C, Jingjing W, Yan X, Dehua L, Liuyin Z and Weihui L 2013 A lateral field excited ZNO film bulk acoustic wave sensor working in viscous environments *J. Micromech. Microeng.* **23** 095032

[19] Doy N, McHale G, Newton M I, Hardacre C, Ge R, MacInnes J M, Kuvshinov D and Allen R W 2010 Small volume laboratory on a chip measurements incorporating the quartz crystal microbalance to measure the viscosity-density product of room temperature ionic liquids *Biomicrofluidics* **4** 014107

[20] Furukawa S, Furukawa H, Nomura T, Yasuda T and Tamura M 1992 Precise estimation of viscosity of liquid using leaky surface acoustic waves propagating along liquid/polymer/$LiNbO_3$ structures *IEEE Ultrasonics Symp. (New York, NY, 20–23 Oct. 1992)* pp 303–6

[21] Sato T, Okajima H, Kashiwase Y, Motegi R and Nakajima H 1993 Shear horizontal acoustic plate mode viscosity sensor *Japan. J. Appl. Phys. 1* **32** 2392–5

[22] Herrmann F, Hahn D and Buttgenbach S 1999 Separate determination of liquid density and viscosity with sagittally corrugated Love-mode sensors *Sensors Actuators* A **A78** 99–107

[23] Martin B A, Wenzel S W and White R M 1990 Viscosity and density sensing with ultrasonic plate waves *5th Int. Conf. on Solid-State Sensors and Actuators and Eurosensors III (Switzerland, 25–30 June 1989)* pp 704–8

[24] Zhou L, Wu Y, Xuan M, Manceau J-F and Bastien F 2012 A multi-parameter decoupling method with a lamb wave sensor for improving the selectivity of label-free liquid detection *Sensors* **12** 10369–80

[25] Anisimkin I V 2003 A novel lamb-mode liquid sensor array *IEEE Ultrasonics Symp. (Piscataway, NJ, 5–8 Oct. 2003)* pp 1326–9

[26] Vellekoop M J, Lubking G W, Sarro P M and Venema A 1994 Evaluation of liquid properties using a silicon Lamb wave sensor *Transducers'93: 7th Int. Conf. on Solid State Sensors and Actuators (Switzerland, 7–10 June 1993)* pp 175–80

[27] Ali R 2010 Time-space analysis of a surface-bonded piezoelectric film's response with lamb wave for diagnostics *Sensors Actuators* A **161** 12–22

[28] Hino R, Esashi M and Tanaka S 2010 Antisymmetric-mode lamb wave methanol sensor with edge reflectors for fuel cell applications *MEMS'10: 23rd IEEE Int. Conf. on Micro Electro Mechanical Systems (Hong Kong, China, 24–28 Jan. 2010)* pp 871–4

[29] Jia H, Duhamel R, Manceau J-F, De Labachelerie M and Bastien F 2005 Improvement of lamb waves sensors: temperature sensitivity compensation *Sensors Actuators* A **121** 321–6

[30] Laurent T, Bastien F O, Pommier J C, Cachard A, Remiens D and Cattan E 2000 Lamb wave and plate mode in ZnO/silicon and AlN/silicon membrane: application to sensors able to operate in contact with liquid *Sensors Actuators* A **87** 26–37

[31] Moll J, Golub M V, Glushkov E, Glushkova N and Fritzen C P 2012 Non-axisymmetric Lamb wave excitation by piezoelectric wafer active sensors *Sensors Actuators* A **174** 173–80

[32] Arapan L, Anderas E, Katardjiev I and Yantchev V 2011 Sensitivity features of thin film plate acoustic wave resonators *IEEE Sensors J.* **11** 3330–1

[33] Yantchev V and Katardjiev I 2013 Thin film lamb wave resonators in frequency control and sensing applications: a review *J. Micromech. Microeng.* **23** 043001

[34] Viktorov I A 1967 *Rayleigh and Lamb Waves: Physical Theory and Applications* (New York: Plenum)

[35] Lin C-M, Chen Y-Y, Felmetsger V V, Vigevani G, Senesky D G and Pisano A P 2012 Micromachined aluminum nitride acoustic resonators with an epitaxial silicon carbide layer utilizing high-order lamb wave modes *MEMS'12: IEEE 25th Int. Conf. on Micro Electro Mechanical Systems (Paris, France, 29 Jan.–2 Feb.)* pp 733–6

[36] Lin C-M, Chen Y-Y, Felmetsger V V, Senesky D G and Pisano A P 2012 AlN/3C-SiC composite plate enabling high-frequency and high-Q micromechanical resonators *Adv. Mater.* **24** 2722–7

[37] Zhou L, Manceau J-F and Bastien F 2009 Influence of gases on lamb waves propagations in resonator *Appl. Phys. Lett.* **95** 223505

[38] Chemical Rubber Company 1998 *CRC Handbook of Chemistry and Physics* (Cleveland, OH: CRC Press)

[39] Jakoby B and Vellekoop M J 1998 Viscosity sensing using a love-wave device *Sensors Actuators* A **68** 275–81

[40] Pantazis A K, Gizeli E and Konstantinidis G 2010 A high frequency GaN Lamb-wave sensor device *Appl. Phys. Lett.* **96** 194103

[41] Kestin J, Khalifa H E and Correia R J 1981 Tables of the dynamic and kinematic viscosity of aqueous NaCl solutions in the temperature range 20–150 °C and the pressure range 0.1–35 MPa *J. Phys. Chem. Ref. Data* **10** 71–87